Experimental and numerical studies on seismic behaviour of exterior beam-column joints

P. Asha[*1] and R. Sundararajan[2]

[1]*Department of Civil Engineering, St. Peter's University, Avadi, Chennai – 54, Tamilnadu, India*
[2]*Government College of Technology, Coimbatore – 13, Tamilnadu, India*

Abstract. A nonlinear finite element analysis using ANSYS is used to evaluate the seismic behavior of reinforced concrete exterior beam-column joints. The behavior of the finite element models under cyclic loading is compared with the experimental results. Two beam-column joint specimens (SH and SHD) with square hoop confinement in joint and throughout the column with detailing as per IS 13920 are studied. The specimen SHD was provided with additional diagonal bars from column to beam to relocate the plastic hinge formation from beam-column interface. The load-displacement relationship, joint shear stress and strain in beam obtained from numerical study showed good agreement with the experimental results. This investigation proves that seismic behaviour of reinforced concrete beam-column joints under reversed cyclic loading can be evaluated successfully using finite element modeling and analysis.

Keywords: reinforced concrete; confinement; beam-column joint; finite element modeling; shear stress

1. Introduction

The failure of several reinforced concrete structures during the recent earthquakes in India as well as in other countries causes concern about the performance of the beam-column joints. The fifth revision of IS 1893 has brought more than 50 percent of the country under moderate and severe seismic zones. Under these circumstances, the detailing of joints assumes more importance. The best layout of reinforcement to give the maximum efficiency in a joint can be evaluated only by actual testing.

In this study, performance of beam-column joints detailed according to the codal recommendations (IS 13920-1993) is evaluated under earthquake loading and an attempt is made to devise superior detailing techniques for improved behaviour of lateral load resisting moment frames.

Several disastrous failures during the 1985 Mexico city earthquake could apparently be attributed to joint failure in cases where heavy spiral or rectilinear confinement in columns above and below a joint was discontinued at the joint (Moehle and Mahin 1991). In general, confinement in columns should continue through the connection region.

Baglin and Scott (2000) investigated the behaviour of exterior beam-column connections under monotonic loading conditions using SBETA, a nonlinear finite element analysis software package

---

∗Corresponding author, Professor, E-mail: asha_panchanathan@yahoo.co.in

developed specifically for the analysis of reinforced concrete structures under plane stress condition. They concluded that the stability of modeling approach was better than some of the more complex packages such that the approach allowed the failure mechanism to be clearly observed with compression zones and dominant tensile cracks clearly indicated.

Li *et al*. (2003) carried out an analytical investigation of seismic behaviour of non-seismically reinforced beam-wide column joints using finite element software. They verified the results from finite element models with that of experimental results and found that there was good agreement between the two. Hegger *et al*. (2004) studied the nonlinear behaviour of reinforced concrete interior and exterior beam-column joints using finite element analysis program ATENA. Details about deformations, cracks and principal compressive strain were obtained from finite element analysis.

Bindhu *et al*. (2010) examined the performance of exterior beam-column joints with non-conventional reinforcement detailing experimentally and analytically. It is observed that the provision of cross diagonal reinforcement increased the ultimate load carrying capacity and ductility of joints.

Zhou and Zhang (2012) derived a formula for calculating the average joint shear from the column shears, and proposed a formula to estimate torque in eccentric exterior beam-column joints induced by seismic action. They also presented numerical results of shear, bending moment and torque in joints induced by seismic action for a pair of concentric and eccentric exterior connections extracted from a seismically designed RC frame. A simplified analysis of the effects of joint shear and torque on the flexural strengths of the critical joint sections is made for the two connections extracted from the frame, and the results indicate that joint shear and torque induced by a strong earthquake may lead to joint-hinging mechanism of seismically designed RC frames.

Rajagopal and Prabavathy (2013) studied and evaluated the performance of beam-column joints with joint detailing as per ACI-352 (mechanical anchorage), ACI-318 (conventional hooks bent) and IS-456(full anchorage conventional hooks bent) along with confinement as per IS-13920 and without confinement. They concluded that significant improvements in seismic performance, ductility and strength were observed while using mechanical anchorage in combination with X-cross bars for less seismic prone areas and X-cross bar plus hair clip joint reinforcement for higher seismic prone areas.

2. Research significance

In this paper, three dimensional finite element models of exterior reinforced concrete beam-column joints (SH and SHD) were developed using ANSYS. The seismic performance of these specimens was evaluated numerically under reversed cyclic loading and a comparison is made with experimental results. There was good agreement between experimental and numerical results in all the parameters compared like load-displacement relationship, joint shear stress and strain in beam. It was found from numerical model of SHD that its plastic hinge formed at a distance of twice the depth of beam from the beam-column interface which was also observed from the experimental results.

3. Details of test specimens

The test specimens were ¼ scale models of typical exterior beam-column joints made up of a single column with one beam in the longitudinal direction. All specimens were cut at mid-height of

supporting column and at midspan of beams, which were the assumed points of inflection. Fig. 1 shows a sketch of test specimens with overall dimensions.

The specimens were designed for both gravity and earthquake forces. The earthquake forces were calculated as per IS 1893-(Part 1) 2002. The specimens were designed for seismic forces and detailed as per IS 13920-1993. The specimen SH (Fig. 2a) had square hoop confinement in the joint which was extended into column which represent the special confining reinforcement as per IS 13920-1993.

The transverse rectangular stirrups made of 3.3 mmϕ mild steel bars were provided at 20 mm c/c from the face of column till a distance of 2D (220 mm) in beam and thereafter at 40 mm c/c according to Clause 6.3.5 of IS 13920. The transverse reinforcement in column spaced at 20 mm c/c was placed to a height of 180 mm above and below the level of joint in the column which was calculated according to Clause 7.4.1 of the code IS 13920. Thereafter, they were provided at 40 mm c/c. The reinforcement details of the test specimens are given in Fig. 2a.

In SHD (Fig. 2b), four inclined bars extend from column to beam, two from the column portion above the joint and two from the column portion below the joint. These four bars were crossed with an aim to relocate the plastic hinge beyond the joint location in the beam region. The percentage of column, beam and joint reinforcement of the test specimens is given in Table 1.

Table 1 Percentage of reinforcement in test specimens

Description	SH	SHD
% of A_{s1b}	1.52	2.54 (up to 2D) 1.52 (beyond 2D)
%of A_{s2b}	1.02	2.03 (up to 2D) 1.02 (beyond 2D)
% of A_{sc}	1.24	3.72 (up to170 mm from beam top and beam bottom) 1.24 (beyond 170 mm)
% of A_{sj}	1.16	1.16

A_{sc} = Area of column reinforcement
A_{s1b} = Area of beam top reinforcement
A_{s2b} = Area of beam bottom reinforcement
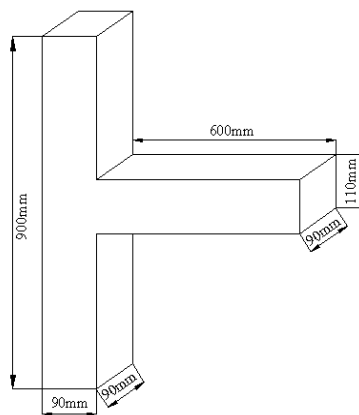A_{sj} = Area of joint reinforcement
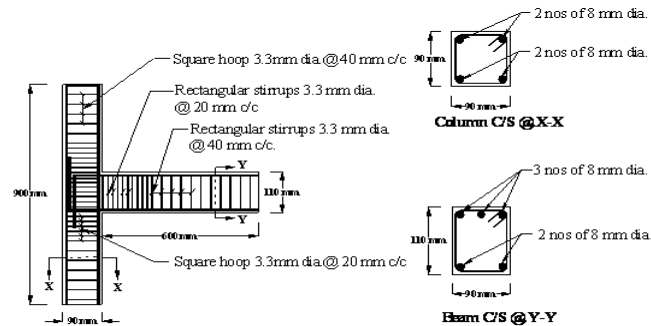

Fig. 1 Overall dimensions of test specimens

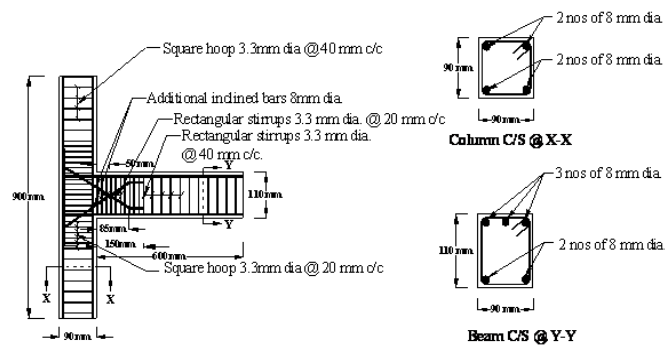Fig. 2(a) Reinforcement details of SH

Fig. 2(b) Reinforcement details of SHD

3.1 Materials

Concrete was made with 43 grade cement, river sand and 6 mm crushed aggregate. The quantities of materials per cubic meter of concrete were as follows

Cement = 412kg
Water/cement ratio = 0.5
Water = 206 litre
Coarse aggregate = 953.09kg
Fine aggregate = 719kg
The 28th day cube compressive strength of the test specimens was 37.52MPa

3.2 Test setup and loading

The specimens were tested with the column portion vertical in a 100 ton reinforced concrete reaction frame as shown in Fig. 3. No axial compression was applied to the columns in order to simulate a worst-case scenario for the joint core. The column ends were attached to pivot assemblies at both ends to provide hinge conditions to simulate point of inflexion at both ends of the column. Screw jacks were placed on top and bottom of beam by which displacement controlled loading was applied. Proving rings were attached to screw jacks which were used to measure the load applied to the beam end. The deflections and rotations of beam were measured by dial gauges.
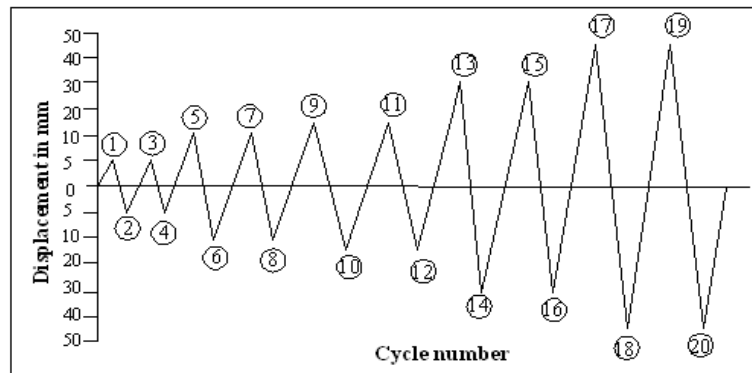
Fig. 3 Test setup

Fig. 4 Cyclic displacement loading

The strain was measured from steel rods which were welded to beam reinforcement by Whittemore strain gauge.

The loading programme consisted of a simple history of reversed symmetric displacement of increasing amplitudes 5 mm,10 mm,15 mm, 30 mm and 45 mm as shown in Fig. 4. The loading in positive direction of first 5 mm displacement cycle was numbered as "1" and the numbering was continued up to the last 45 mm displacement cycle. The first cycle (positive and negative) of 5 mm displacement was numbered as 1 and 2 and second cycle (positive and negative) of 5 mm displacement was numbered as 3 & 4 as shown in Fig. 4. Remaining cycles of displacement were numbered consecutively as shown in Fig. 4.

During each cycle the loading was temporarily stopped at Y/4 mm displacement intervals where "Y" is the peak displacement value for a cycle so as to enable the readings from dial gauges and proving ring to be noted. The readings from strain points were also noted only at peak displacement values.

4. Numerical study

4.1 Element types

The requirement to include nonlinear response of reinforced concrete in capturing the ultimate response of reinforced structures demands the use of dedicated Solid 65 element. The rebar capability of Solid 65 element was turned off in finite element models and the element has eight nodes, each having three translation degrees of freedom. Discrete modeling of reinforcement was adopted in this study which was also found to be the best strategy for modeling of reinforcement (Wolanski 2004).

Link 8 element was used to model the steel reinforcement in the finite element models of exterior beam-column joint specimens. This element is a 3D spar element and it has two nodes with three degrees of freedom-translations in the nodal x, y, and z directions.

Solid 65 element requires linear isotropic and multilinear isotropic material properties to properly model concrete. The multilinear isotropic material uses the William and Warnke (1974) model to define the failure of the concrete. Poisson's ratio (ν) of concrete was assumed as 0.15. The cube compressive strength of concrete (f_{ck}) used for calculation of E_c and f_{cr} and ultimate uniaxial compressive strength of concrete cylinders ($f_c^{'}$) used for calculation of ultimate strain were based on the experimental results.

The compressive uniaxial stress-strain relationship for the concrete model was obtained using the following equations to compute the multi-linear isotropic stress-strain curve for Solid 65 element (Desayi and Krishnan 1964, MacGregor 1992).

$$f = \frac{E_c \varepsilon}{1 + \left(\dfrac{\varepsilon}{\varepsilon_0} \right)^2} \tag{1}$$

$$\varepsilon_o = \frac{2f_c^{'}}{E_c} \tag{2}$$

$$E_c = \frac{f}{\varepsilon} \tag{3}$$

where 'f' is the stress at any strain 'ε' and ε_0 is the strain at the ultimate compressive strength ($f_c^{'}$).

The modulus of elasticity of concrete (E_c) and uniaxial cracking stress (f_{cr}) were based upon definitions proposed by IS 456-2000. These values were determined using equations,

$$E_c = 5000 \sqrt{f_{ck}} \tag{4}$$

$$f_{cr} = 0.7 \sqrt{f_{ck}} \tag{5}$$

The Link 8 element used for main and transverse steel reinforcement was assumed to be bilinear isotropic. Bilinear isotropic material was based on the von Mises failure criteria. The yield stress for main and transverse steel reinforcement and welded wire mesh used in finite element models was based on experimental results. The modulus of elasticity of steel used was 200000 MPa which was taken from experimental result and Poisson's ratio was assumed as 0.3.

Shear transfer coefficients range from 0.0 to 1.0, with 0.0 representing a smooth crack (complete loss of shear transfer) and 1.0 representing a rough crack (no loss of shear transfer). Shear transfer coefficient for the open crack (β_t) was set to 0.3 in this study. A value of 0.8 was adopted for shear transfer coefficient for closed crack based on trial and error with which no convergence problems were encountered.

The Newton-Raphson method of analysis was used to compute the nonlinear response. Newton-Raphson equilibrium iterations provide convergence at the end of each load increment within tolerance limits. The maximum number of equilibrium iterations was given a value of 1000. Line search method was used in the nonlinear analysis for accelerating the convergence.

4.2 Finite element discretization

In the finite element modeling of reinforced concrete structures, it is important to select an appropriate mesh size to meet the requirement of accuracy and computation speed.

The beam and column portions of all the finite element models were created as single volume and meshing was performed using volume sweep option in order to maintain consistency of width and length of concrete elements of column with that of elements and nodes of beam at the beam-column joint interface. The global mesh size of concrete elements was 20 mm. The steel and welded wire mesh reinforcement was also meshed as 20 mm long line elements. The total number of concrete (Solid 65) elements in the finite element models of exterior beam-column joint specimens was 2050.

On average the total number of Link 8 elements in the finite element models was 1355. Figs. 5 and 6 illustrate the mesh of concrete and steel portions of finite element model of exterior beam-column joint specimen of SH. The dimensions, reinforcement details and reversed cyclic loading history of finite element models were same as that of actual test specimens.

5. Results and discussion

5.1 Hysteresis behaviour

The force-displacement hysteretic loops of SH and SHD are shown in Fig. 7(a) and (b) respectively. The ultimate loads of SH and SHD were 10kN and 13.25kN respectively. Fig. 7(a) shows that only slight pinching of loop was observed in SH as displacement progressed which may be attributed to hairline diagonal shear cracks in the joint region. From Fig. 7(b) it is seen that the lateral load-displacement relation curve of SHD was very stable and there was no pinching in the curve. The four additional inclined bars provided from column to beam prevented the joint from diagonal shear cracks and shifted the plastic hinge from the beam-column interface to a distance of 2D from the face of column.

5.2 Numerical load-displacement behaviour

The comparison between experimental and numerical load-displacement envelope curves for SH and SHD series are shown in Figs. 8(a) and (b) respectively. There was good agreement between the two curves for both the specimens. The numerical maximum load (P_{ANSYS}) for SH and SHD was 11.5kN and 13.5kN respectively. The numerical maximum load (P_{ANSYS}) of SH and SHD was greater than the experimental maximum load (P_{Exp}) by 10% and 7.5% respectively.
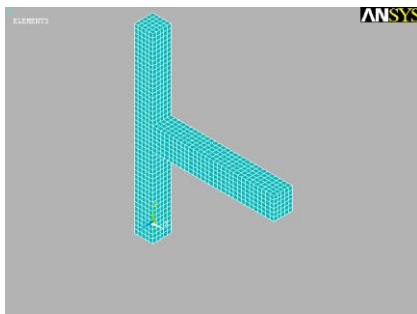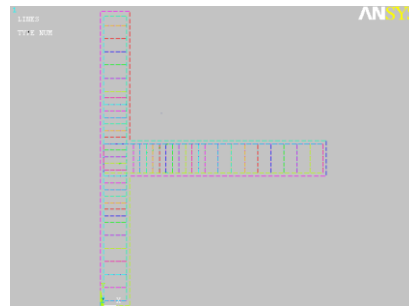

Fig. 5 Finite element mesh of concrete
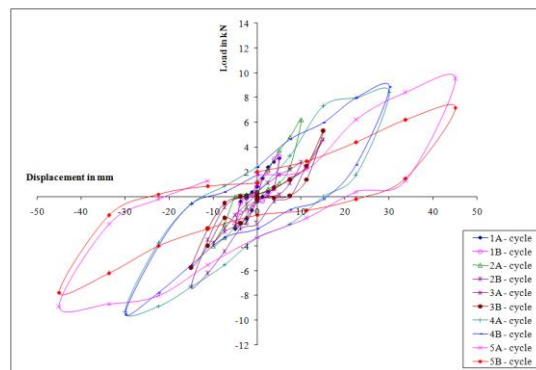

Fig. 6 Finite element mesh of reinforcement
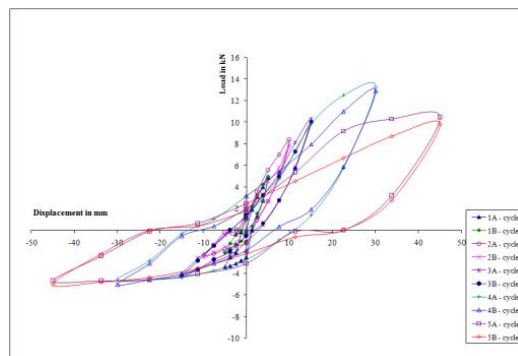

Fig. 7(a) Hysteresis loop of SH

Fig. 7(b) Hysteresis Loop of SHD

5.3 Displacement ductility

The term displacement ductility is defined as the ratio between maximum displacement (Δ_{max}) to the displacement at first yield (Δ_y). The ductility of SHD was 8.57 and that of SH was only 6.

5.4 Energy dissipation

The effectiveness of any detailing scheme is in the amount of energy dissipated by the structural component provided with such a detailing scheme (Murty *et al*. 2001). The energy dissipated during a particular loading cycle is computed as the area enclosed within the load versus displacement curve, starting and ending with a zero displacement (Alameddine and Ehsani 1991). The cumulative energy dissipated (E_t) versus displacement curves of SH and SHD is shown in Fig. 9. The cumulative energy dissipated by SHD was 9% greater than that of SH.
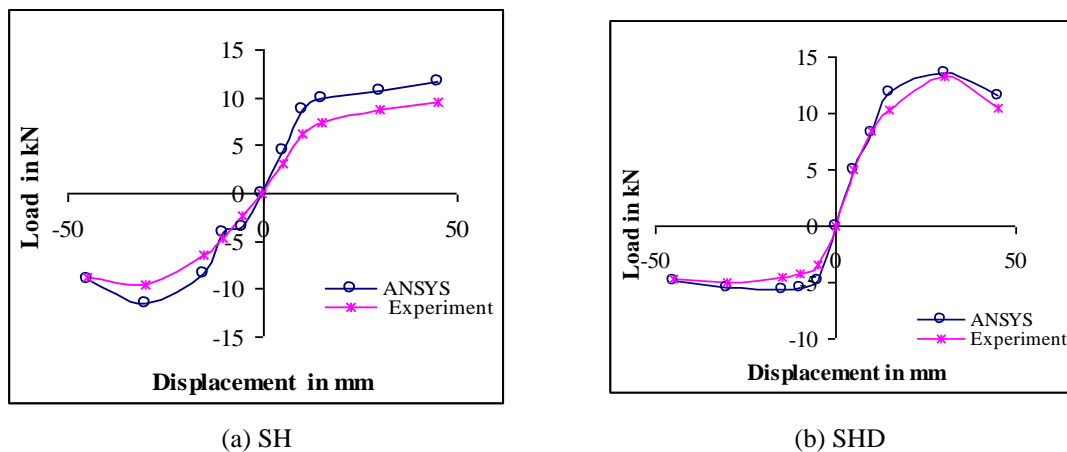
(a) SH   (b) SHD

Fig. 8 Load-displacement envelope curves
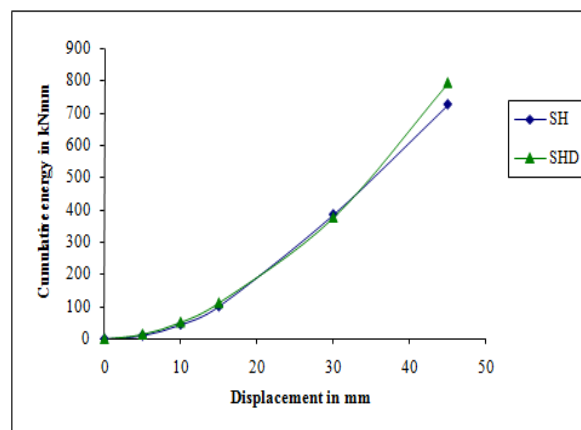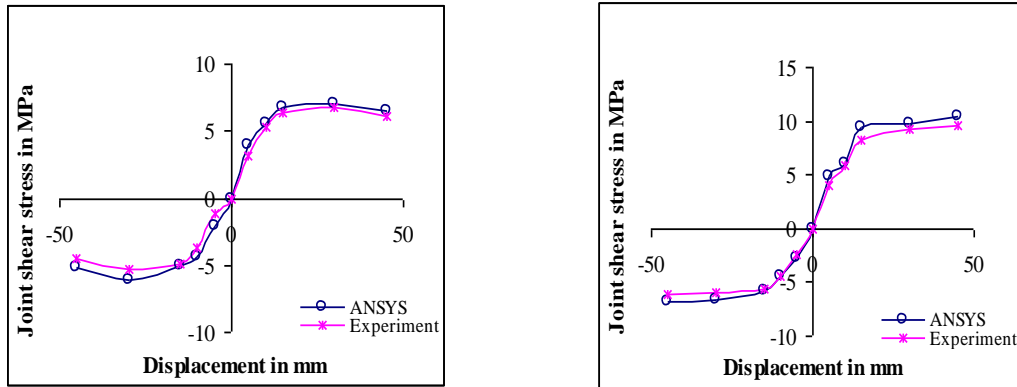
Fig. 9 Cumulative energy versus displacement curves

(a) SH   (b) SHD

Fig. 10 Horizontal joint shear stress versus displacement curves

Table 2 Beam rotation

Specimen	Beam rotation at a distance of D in radian	Beam rotation at a distance of 2D in radian
SH	0.123	0.09
SHD	0.063	0.075

5.5 Numerical horizontal joint shear stress versus displacement behaviour

The numerical horizontal joint shear stress was obtained from shear stress contour in the XZ direction for the specimens and shear stress (τ_{ANSYS})from two displacement cycles of equal magnitude are averaged and plotted in both the directions of loading. The numerical joint shear stress versus displacement curves are compared with the experimental results. Figs. 10(a) and (b) shows the shear stress contour in the XZ direction of SH and SHD respectively. It is observed that SH experienced a reduction in their shear stress after 30 mm displacement cycle and SHD showed rising trend in the shear stress up to the last displacement cycle. The maximum value of numerical joint shear stress (τ_{ANSYS}) sustained by specimens SH and SHD was greater than their corresponding experimental shear stress values by 9% and 6% respectively.

5.6 Beam rotation

Dial gauges were used to derive beam rotations θ_D and θ_{2D} at distances of D and 2D from the column face of the beam respectively. If the beam rotation at a distance of 2D is larger than beam rotation at D, it indicates the development of plastic hinge is away from the column face.

SHD had its beam rotation θ_{2D} greater than θ_D. It is seen from Table 2 that θ_D and θ_{2D} at 45 mm displacement of SHD were 0.063 and 0.075 radian respectively. The beam rotation at a distance of 2D of SHD was 16% greater than the rotation at D.

5.7 First principal stress distribution

When the maximum first principal (tensile) stress (σ_1) exceeds the ultimate tensile strength of the concrete, a crack plane will form, the normal stiffness component to the crack plane is released, and the shear components of the crack plane are reduced (Eshghi and Farrokhi 2003). Thus the regions in exterior beam-column joint specimens undergoing excessive cracking can be identified from numerical models where the peak value of first principal stress exceeded the ultimate tensile strength of concrete.

The first principal stress contour for the specimens at last displacement cycle was captured from ANSYS analysis and regions of excessive cracking are compared with those obtained from experiment. The ultimate tensile strength of SH and SHD was 2.38 MPa and 2.86 MPa respectively.

The first principal stress distribution of specimens SH and SHD at last displacement cycle is shown in Figs. 11(a) and (b) respectively. From the finite element models of SH and SHD, it is seen that red colour appears at the beam-column interface which indicates maximum first principal stress in that region.

The peak principal tensile stress of SH and SHD was 13.25MPa and 19 MPa respectively. Hence it can be inferred that severe cracks were developed only at the interface in both the specimens. Minor cracks were observed in the joint region of SH whereas the joint region was completely safe against failure in SHD and the tensile stress exceeding the tensile strength of concrete spread only in the beam region. Thus crack pattern from the experiments of the test specimens was accurately predicted by the respective finite element models developed through the concrete first principal stress distribution contour plots.

5.8 Third principal strain distribution

The location of maximum strain in the beams corresponds to the centre of the plastic hinging zone (Fattah and Wight 1987). The location of maximum third principal strain ε_3 in the numerical models of beam-column joint specimens indicates the location of plastic hinge in beam.

(a) SH   (b) SHD

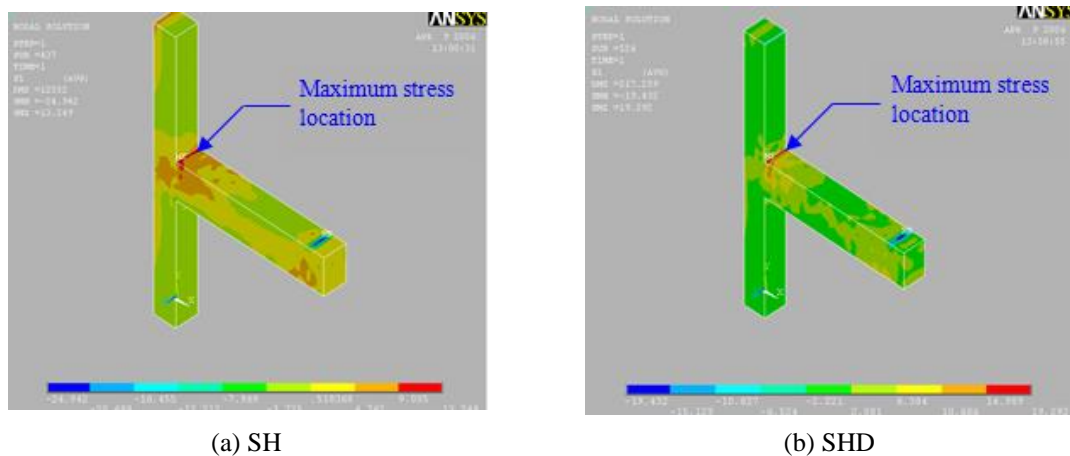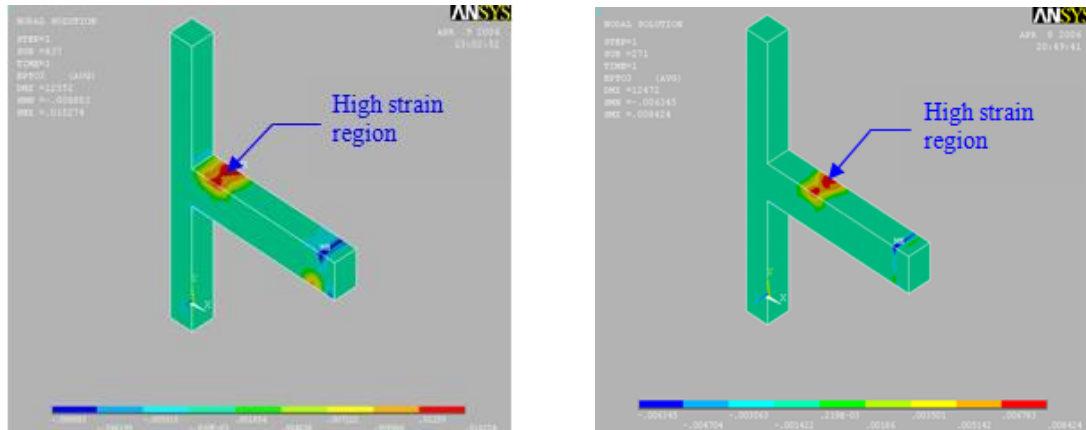Fig. 11 Contour plots of concrete first principal stress in concrete

(a) SH   (b) SHD

Fig. 12 Contour plots of third principal strain in concrete

(a) SH   (b) SHD

Fig. 13 Crack pattern

The concrete third principal strain contour of finite element models were captured at last displacement cycle and the location of maximum strain which denotes location of plastic hinges is discussed in this section. High strain point is always denoted in red colour in the third principal strain contour also.

The third principal strain contour of specimens SH and SHD are shown in Figs. 12(a) and (b) respectively.

From the contour of SH, it was observed that high strain value of 0.0152 occurred at a distance of 0.75 D from the column face. This indicates that the plastic hinge has formed within a distance of D from the column face and was distributed over a considerable region of the beam. Third principal strain distribution of SHD shown in Fig. 12(b) illustrates that a peak third principal strain of 0.0084 occurred at a distance of 2D away from the beam-column interface. The additional inclined bars in SHD from the column to beam have shifted the plastic hinge zone from the joint region to a distance greater than D from the face of the column.

5.9 Crack pattern

The crack pattern of SH and SHD are shown in Figs. 13(a) and (b) respectively. SH had diagonal tension cracks in both the directions which resulted in 'X' shaped cracks in the joint region. The vertical flexure crack at the beam-column interface extended as through-depth crack indicating the formation of plastic hinge.

From Fig. 13(b), it is seen that SHD experienced hairline 'X' shaped cracks in the joint region and full depth cracks in beam region approximately at a distance of 2D from the face of column. This has confirmed that the plastic hinge has formed in the beam is approximately at the location where the additional inclined bars were curtailed.

6. Conclusions

Three dimensional finite element models of beam-column joint specimens were developed using ANSYS and the seismic behaviour of beam-column joint specimens was assessed numerically and experimentally. From the experimental results it is observed that SHD performed better than SH in all the aspects. Load carrying capacity, energy dissipation and displacement ductility of SHD was higher than that of SH by 32%, 9% and 43% respectively. Plastic hinge formation was also shifted to approximately 2D distance from beam-column interface in SHD as expected which was confirmed from the beam rotation and crack pattern.

It is found that finite element modeling can be effectively used for nonlinear analysis of reinforced concrete exterior beam-column joints subjected to reversed cyclic loading. The finite element results agreed well with experimental results and following are the most important conclusions:

• The numerical maximum load and horizontal joint shear stress was higher than the corresponding values from experimental results by 9% and 7.5% respectively.

• The regions of excessive cracking obtained from first principal stress distribution of the finite element models correspond well with the regions of severe damage observed from the experimental crack pattern of beam-column joint specimens.

• The location of maximum strain region from third principal strain distribution of finite element models coincided with the corresponding locations of test specimens. This indicates that finite element models simulate the exact seismic behaviour of test specimens.

Reference

Alameddine, F. and Ehsani, M.R. (1991), "High strength RC connections subjected to inelastic cyclic loading", *ASCE J. Strcut. Eng.*, **117**(3), 829-850.

Baglin, P.S. and Scott, R.H. (2000), "Finite element modeling of reinforced concrete beam-column connections", *ACI Struct. J.*, **97**(6), 886-894.

Bindhu, K.R. and Jaya, K.P. (2010), "Strength and behaviour of exterior beam-column joints with diagonal crossing bars", *Asian J. Civil Eng.*, **11**(3), 397-410.

Desayi, P. and Krishnan, S., (1964), "Equation for the stress-strain curve of concrete", *ACI Struct. J.*, **61**, 345-350.

Eshghi, S. and Farrokhi, H. (2003), "Seismic vulnerability analysis of airport traffic control towers", *J. Seismol. Earthq. Eng.*, Spring, **5**(1), 31-40.

Fattah, B.A. and Wight, J.K. (1987), "Study of moving beam plastic hinging zones for earthquake-resistant design of R/C buildings", *ACI Struct. J.*, **84**(1), 31-39.

Hegger, J., Sheriff, A. and Roeser, W. (2004), "Nonlinear finite element analysis of reinforced concrete beam-column connections", *ACI Struct. J.,* **10**(5), 604-614.

Li B, Wu, Y. and Tso, C.P. (2003), "Seismic behavior of non-seismically detailed interior beam-wide column joints-part II: theoretical comparisons and analytical studies", *ACI Struct. J.*, **100**(1), 56-65.

Murty, C.V.R., Rai, D.C., Bajpai, K.K. and Jain, S.K. (2003), "Anchorage details and joint design in seismic RC frames", *The Indian Concrete J.*, **75**(4), 274-280.

Rajagopal, S. and Prabavathy, S. (2013), "Study of exterior beam-column joint with different joint core and anchorage details under reversal loading", *Struct. Eng. Mech.*, **46**(6), 809-825.

Zhou, H. and Zhang, Z. (2012), "Interaction of internal forces of exterior beam-column joints of reinforced concrete frames under seismic action", *Struct. Eng. Mech.*, **44**(2), 197-217.

MacGregor, J**.** (1992), *Reinforced Concrete Mechanics and Design*, Third Edition, Prentice Hall, Upper Saddle River, New Jersey

Moehle, J.P. and Mahin, S.A. (1991), "Observations on the behavior of reinforced concrete buildings during earthquakes", *Earthquake-Resistant Concrete Structures Inelastic Response and Design SP-127*, American Concrete Institute, S.K. Ghosh (Editor), Detroit, Michigan, 67-89.

William, K.J. and Warnke, E.P. (1974), "Constitutive model for triaxial behaviour of concrete", Seminar on concrete structures subjected to triaxial stresses, *International Association of Bridge and Structural Engineering Conference*, Bergamo, Italy.

Wolanski, A.J. (2004), "Flexural Behavior of Reinforced and Prestressed Concrete Beams using Finite Element Analysis", Master's Thesis, Marquette University, Milwaukee, Wisconsin.

IS 13920 (1993), *Indian Standard Ductile Detailing of Reinforced Concrete Structures Subjected to Seismic Forces-Code of Practice,* New Delhi..

IS 1893 (Part 1) (2002), *Indian Standard Criteria for Earthquake Resistant Design of Structures, Part-1, General Provisions and Buildings,* New Delhi..

IS 456 (2000), *Indian Standard Plain and Reinforced Concrete Code of Practice*, New Delhi.

ANSYS10.0 (1995), *ANSYS Users manual*, (ANSYS, Inc.), Canonsburg.

CC